Computational and Structural Biotechnology Journal 21 (2023) 665–676

Contents lists available at ScienceDirect

Computational and Structural Biotechnology Journal

journal homepage: www.elsevier.com/locate/csbj

Single-cell analysis of multiple cancer types reveals differences in endothelial cells between tumors and normal tissues

Jiayu Zhang [a,1], Tong Lu [a,1], Shiqi Lu [b,1], Shuaijun Ma [a], Donghui Han [a], Keying Zhang [a], Chao Xu [a], Shaojie Liu [a], Lunbiao Gan [b], Xinjie Wu [b], Fa Yang [a,*], Weihong Wen [b,**], Weijun Qin [a,*]

[a] Department of Urology, Xijing Hospital, Air Force Medical University, Xi'an, China
[b] Institute of Medical Research, Northwestern Polytechnical University, Xi'an, China

ARTICLE INFO

Article history:
Received 9 October 2022
Received in revised form 28 December 2022
Accepted 29 December 2022
Available online 30 December 2022

Keywords:
Tumor microenvironment
Endothelial cells
Single-cell RNA sequencing

ABSTRACT

Endothelial cells (ECs) play an important role in tumor progression. Currently, the main target of anti-angiogenic therapy is the vascular endothelial growth factor (VEGF) pathway. Some patients do benefit from anti-VEGF/VEGFR therapy; however, a large number of patients do not have response or acquire drug resistance after treatment. Moreover, anti-VEGF/VEGFR therapy may lead to nephrotoxicity and cardiovascular-related side effects due to its action on normal ECs. Therefore, it is necessary to identify targets that are specific to tumor ECs and could be applied to various cancer types. We integrated single-cell RNA sequencing data from six cancer types and constructed a multi-cancer EC atlas to decode the characteristic of tumor ECs. We found that tip-like ECs mainly exist in tumor tissues but barely exist in normal tissues. Tip-like ECs are involved in the promotion of tumor angiogenesis and inhibition on anti-tumor immune responses. Moreover, tumor cells, myeloid cells, and pericytes are the main sources of pro-angiogenic factors. High proportion of tip-like ECs is associated with poor prognosis in multiple cancer types. We also identified that prostate-specific membrane antigen (PSMA) is a specific marker for tip-like ECs in all the cancer types we studied. In summary, we demonstrate that tip-like ECs are the main differential EC subcluster between tumors and normal tissues. Tip-like ECs may promote tumor progression through promoting angiogenesis while inhibiting anti-tumor immune responses. PSMA was a specific marker for tip-like ECs, which could be used as a potential target for the diagnosis and treatment of non-prostate cancers.

© 2022 The Authors. Published by Elsevier B.V. on behalf of Research Network of Computational and Structural Biotechnology. This is an open access article under the CC BY-NC-ND license (http://creativecommons.org/licenses/by-nc-nd/4.0/).

1. Introduction

Tumor blood vessels facilitate tumor progression through multiple mechanisms. Tumor vasculature provides oxygen and nutrients for tumor growth [1]. Compared with normal blood vessels, the tumor vasculature is highly leaky, tortuous, and disorganized, which promotes solid tumor growth and metastasis [2]. Tumor blood vessels also contribute to the acquisition of cancer stem cell (CSC) characteristics [3]. More importantly, tumor blood vessels not only directly promote tumor growth and metastasis, they also play a role in immune escape. In tumor microenvironment (TME), endothelial cells (ECs) may disrupt antitumor immune response by influencing the infiltration of immune cells [4–8].

Currently, the main target of anti-angiogenic therapy is the vascular endothelial growth factor (VEGF) pathway. Some patients do benefit from anti-VEGF/VEGFR therapy, especially in renal cell

Abbreviations: ECs, Endothelial cells; scRNA-seq, Single-cell RNA sequencing; PSMA, Prostate-specific membrane antigen; VEGF, Vascular endothelial growth factor; TME, Tumor microenvironment; CRC, Colorectal cancer; PDAC, Pancreatic ductal adenocarcinoma; GC, Gastric cancer; LC, Lung cancer; OVC, Ovarian cancer; RCC, Renal cell carcinoma; BRCA, Breast invasive carcinoma; CESC, Cervical squamous cell carcinoma and endocervical adenocarcinoma; HNSC, Head and Neck squamous cell carcinoma; KICH, Kidney chromophobe; KIRC, Kidney renal clear cell carcinoma; KIRP, Kidney renal papillary cell carcinoma; LIHC, Liver hepatocellular carcinoma; LUAD, Lung adenocarcinoma; LUSC, Lung squamous cell carcinoma; OV, Ovarian serous cystadenocarcinoma; PAAD, Pancreatic adenocarcinoma; PRAD, Prostate adenocarcinoma; READ, Rectum adenocarcinoma; STAD, Stomach adenocarcinoma

* Correspondence to: Department of Urology, Xijing Hospital, Air Force Medical University, 127 Changle West Road, Xi'an, China.
** Correspondence to: Institute of Medical Research, Northwestern Polytechnical University, 127 West Youyi Road, Xi'an, China.
E-mail addresses: yangfa@fmmu.edu.cn (F. Yang), weihongwen@nwpu.edu.cn (W. Wen), qinwj@fmmu.edu.cn (W. Qin).
[1] These authors contributed equally to this work.

https://doi.org/10.1016/j.csbj.2022.12.049
2001-0370/© 2022 The Authors. Published by Elsevier B.V. on behalf of Research Network of Computational and Structural Biotechnology. This is an open access article under the CC BY-NC-ND license (http://creativecommons.org/licenses/by-nc-nd/4.0/).

carcinoma (RCC), colorectal cancer (CRC), and glioblastoma multiforme [9,10]. However, a large number of patients do not respond or develop resistance after treatment [9,11]. This could be caused by the reason that tumor tissues can produce alternative angiogenic growth factors to stimulate angiogenesis and ensure blood flow [12]. Moreover, anti-VEGF/VEGFR therapy could also play a role on normal ECs, and, thus increased nephrotoxicity and cardiovascular side effects, such as hypertension and thromboembolic events [13]. Therefore, it is necessary to identify tumor EC specific targets, which are applicable to various cancer types.

ECs are composed of distinct subclusters [14–16]. Decoding the differences between tumor ECs and normal ECs could facilitate the development of more effective diagnostic and therapeutic strategies. We aimed to identify tumor-specific EC subclusters and to find out novel specific targets. Thus, in this study, we constructed a multi-cancer EC atlas and examined the differences between tumor and normal tissue ECs by integrated analysis of single-cell RNA-sequencing (scRNA-seq) data from various cancer types.

2. Methods

2.1. Collection of scRNA-seq data for multiple cancer types

We performed a dedicated literature search on scRNA-seq studies of human cancer published in last three years and had publicly available data. We selected the scRNA-seq data which included all cell types of both tumor tissues and normal tissues. Then, we collected scRNA-seq data from six human cancer types, including CRC, gastric cancer (GC), lung cancer (LC), ovarian cancer (OVC), pancreatic ductal adenocarcinoma (PDAC), and RCC [17–20]. The number of cells from each cancer type was similar in order to avoid an excessive number of ECs from a single cancer type, which may mask the common features of multi-cancer ECs. The sources and sample information for the scRNA-seq data are presented in Table S1.

2.2. Integrated analysis of multi-cancer scRNA-seq data

We updated the gene symbols of all scRNA-seq gene expression matrices through HGNChelper package. We used the Seurat package (v4.0.5) to analyze the scRNA-seq data [21]. First, we generated six Seurat Objects using the gene expression matrices of individual cancer types in Seurat. Second, we filtered these Seurat Objects to exclude cells with fewer than 200 genes, more than 8000 genes, more than 25 % mitochondrial genes, and greater than 1 % hemoglobin genes. Third, we merged all the Seurat Objects to construct a combined Seurat Object. The merged Seurat Object was normalized and scaled separately using the NormalizeData and ScaleData functions. Variable genes were identified using the Find Variable Features function. 2000 variable genes were used for downstream analysis. We applied the RunPCA function to conduct principal component analysis (PCA). After PCA, the RunHarmony function of the Harmony package (v0.1.0) was used to integrate the Seurat Object and correct batch effects from different samples [22]. The sample number was selected as the variable for batch correction, and the default parameters were used for other settings. Finally, we performed clustering using the Find Neighbors and Find Clusters functions at a resolution of 3. We used 50 principal components for the analyses. Uniform manifold approximation and projection (UMAP) was then applied to visualize the cell atlas.

We identified different genes in cell clusters using the Find All Markers function via Wilcoxon rank-sum tests. Each cell cluster was then identified as the specific cell type according to classical marker genes as follows: B cells (marked using CD79A and MS4A1), plasma cells (marked using CD79A, IGHA1, and IGLC2), $CD4^+$ T cells (marked using CD3D, CD4, and IL7R), $CD8^+$ T cells (marked using CD3D, CD8A, and CD8B), dendritic cells (DCs, marked using PTPRC and CD1C), ECs (marked using PECAM1 and vWF), epithelial cells (marked using EPCAM and KRT8), fibroblasts (marked using COL1A1 and DCN), macrophages (marked using CD68 and MARCO), mast cells (marked using CPA3 and KIT), monocytes (marked using CD14 and S100A8), natural killer cells (NK cells, marked using NKG7 and GNLY), and pericytes (marked using RGS5, ACTA2, and CSPG4).

2.3. Construction of the multi-cancer EC atlas

We extracted EC data from the multi-cancer scRNA-seq dataset. The Harmony package was then applied to integrate the scRNA-seq data of ECs. ECs of multiple cancers were then classified into six distinct subclusters. Visualization of the EC atlas was implemented using the UMAP method.

2.4. Gene set variation analysis

Gene set variation analysis (GSVA) was performed using the GSVA package (v1.40.1) [23]. Specifically, single-sample gene set enrichment analysis (ssGSEA) was applied to identify the enriched pathways of Gene Ontology (GO) terms and 50 hallmark gene sets from the Molecular Signatures Database (MSigDB) for each cell.

2.5. Cell-cell communication analysis

The CellChat package (v1.1.3) was used to identify cell-cell interactions according to the expression of known ligand-receptor pairs in different cell clusters [24]. An official workflow was used to perform further analyses. The reference database used for ligand-receptor pairs was “Secreted Signaling” from CellChatDB.human. Primary analysis was completed using the following essential functions: “identifyOverExpressedGenes” with thresh.p = 0.05, “identifyOverExpressedInteractions,” “computeCommunProb,” “computeCommunProbPathway” with thresh = 0.05, and “aggregateNet” with thresh = 0.05. The result of cell-cell communication was visualized using the “netVisual_bubble” function with remove.isolate = FALSE.

2.6. Cell composition deconvolution

Cell composition deconvolution was performed using CIBERSORTx [25]. First, we constructed a signature gene expression matrix based on the multi-cancer scRNA-seq dataset. We extracted raw count matrix and cell type information from a subset of the Seurat object, including 200 of each EC subcluster and 500 of each other cell type. The raw count matrix was imported in CIBERSORTx and normalized. The signature matrix in CPM (counts per million) was generated using CIBERSORTx. All genes were used to generate the signature gene expression matrix. The signature gene expression matrix included 4556 genes (Table S8). Second, we transformed fragments per kilobase of transcript per million mapped reads (FPKM) values of TCGA bulk RNA-seq data into transcripts per million reads (TPM) values. Finally, the cell proportions of TCGA samples were evaluated using CIBERSORTx, based on bulk RNA-seq data. We performed batch correction with S-mode to correct for the cross-platform variation in the deconvolution of TCGA RNA-seq data. TCGA datasets used in this study included the RNA-seq data and survival data of Bladder urothelial carcinoma (BLCA), Breast invasive carcinoma (BRCA), Cervical squamous cell carcinoma and endocervical adenocarcinoma (CESC), Colon adenocarcinoma (COAD), Esophageal carcinoma (ESCA), Glioblastoma multiforme (GBM), Head and Neck squamous cell carcinoma (HNSC), Kidney Chromophobe (KICH), Kidney renal clear cell carcinoma (KIRC), Kidney renal papillary cell carcinoma (KIRP), Liver hepatocellular carcinoma (LIHC), Lung adenocarcinoma (LUAD), Lung squamous cell carcinoma (LUSC), Ovarian serous cystadenocarcinoma (OV), Pancreatic adenocarcinoma

(PAAD), Prostate adenocarcinoma (PRAD), Rectum adenocarcinoma (READ), Stomach adenocarcinoma (STAD), Thyroid carcinoma (THCA), and Uterine corpus endometrial carcinoma (UCEC). The cell types included arterial ECs, venous ECs, capillary ECs 1, capillary ECs 2, tip-like ECs, lymphatic ECs, B cells, $CD4^+$ T cells, $CD8^+$ T cells, DCs, ECs, epithelial cells, macrophages, mast cells, monocytes, NK cells, and pericytes.

To examine the accuracy of tip-like EC proportion calculated by deconvolution, we analyzed the correlation between enrichment score of tip-like EC gene signature and tip-like EC proportion in multiple cancer types. First, we screened the specific markers of tip-like ECs. Then, in order to construct the tip-like EC gene signature, we intersected the EC marker genes ($\log_2$ FoldChange > 1.5, $p < 0.05$) with the top 30 genes that were highly expressed in tip-like ECs compared with other EC subclusters. Tip-like EC gene signature included COL4A1, COL4A2, ESM1, SPARC, INSR, IGFBP3, HTRA1, VWA1, COL15A1, PLVAP, ANGPT2, HSPG2, EDNRB, RGCC, and IGFBP7. Second, we performed GSVA for tip-like EC gene signature in bulk RNA-seq data of TCGA cancer samples. Finally, we performed correlation analysis to examine the correlation between the score of tip-like EC gene signature and tip-like EC proportion calculated by deconvolution.

2.7. Survival analysis

Survival analysis of distinct EC subclusters was performed using the R packages survival (v3.2.13) and survminer (v0.4.9). Patients in each TCGA cancer cohort were divided into tip EC-high (top quarter) and tip EC-low (bottom quarter) groups based on the proportions of tip-like ECs. We then applied the "survfit" function to generate Kaplan-Meier survival plots for individual cancer types.

2.8. Statistical analysis

Statistical analyses were performed using R software (v4.1.2). The Wilcoxon rank-sum test was used to test the significance of most cases. Statistical significance was defined as $p < 0.05$ ($^*p < 0.05$, $^{**}p < 0.01$, $^{***}p < 0.001$, $^{****}p < 0.0001$; ns, not significant). Overall survival analysis was analyzed using the log-rank test.

3. Results

3.1. Construction of multi-cancer cell atlas

A graphic flowchart summarizing the main process of the study was shown in Fig. 1. We collected scRNA-seq data from six cancer types, including CRC, GC, LC, OVC, PDAC, and RCC (Table S1) [17–20]. Then we performed integrated analysis of the scRNA-seq data and constructed a multi-cancer cell atlas, which included 220,075 high-quality cells from 83 tumor samples and 30 normal tissues, with batch effects across different samples being removed by Harmony package (Fig. 2A, B; Table S1). Cells were divided into 13 distinct cell clusters based on their representative classification markers: B cells, plasma cells, $CD4^+$ T cells, $CD8^+$ T cells, DCs, ECs, epithelial cells, fibroblasts, macrophages, mast cells, monocytes, NK cells, and pericytes (Fig. 2C-E; Fig. S1; Table S2; Table S3).

3.2. Integrated analysis of single-cell and bulk RNA-seq data reveals the differences in EC composition between tumor and normal tissues

We extracted ECs from the multi-cancer cell atlas, and re-clustered them to construct a multi-cancer EC atlas (Fig. S2). In this atlas, 10,277 ECs were classified into six subclusters: arterial ECs (marked by GJA5, FBLN5, and LTBP4), venous ECs (marked by ACKR1, SELP, and VCAM1), capillary ECs 1 (marked by CA4, FCN3, and EDN1), capillary ECs 2 (marked by CA4 and EMCN), tip-like ECs (marked by CXCR4, ESM1 and ANGPT2), and lymphatic ECs (marked by PROX1) (Fig. 3A-D; Fig. S3A; Table S4) [15,26,27]. Capillary ECs 1 and capillary ECs 2 expressed CA4, the classical marker for capillary ECs (Fig. 3A). Capillary ECs 1 exist in various tissues, while capillary ECs 2 mainly exist in kidney and may be a tissue-specific EC subcluster (Fig. 3D; Fig. S3C). We found that tip-like ECs mainly existed in tumor tissues in all the cancer types we studied, while barely existed in normal tissues. Other subclusters didn't show such difference between tumor tissues and normal tissues in multiple cancer types (Fig. 3B, D; Fig. S3B, C; Table S5).

We further assessed the proportion of EC subclusters in multiple TCGA cohorts (Table S6; Table S7). Cell-type deconvolution analysis was performed using CIBERSORTx with the scRNA-seq data of multiple cancer types as a reference panel (Fig. S4A, B; Table S8). To examine the accuracy of the tip-like EC proportion calculated by deconvolution, we analyzed the correlation between the enrichment score of tip-like EC gene signature and proportion of tip-like ECs in multiple cancer types. We found a positive correlation between gene signature and proportion of tip-like ECs, indicating that the prediction of tip-like EC proportion was based on the specific gene expression in tip-like ECs (Fig. S4A). Results also showed that the proportion of tip-like ECs was significantly higher in tumor tissues than normal tissues in most cancer types (16 out of 20), which was consistent with the results of multi-cancer scRNA-seq data (Fig. 3E; Table S9). Similarly, proportions of three EC clusters, including arterial ECs, venous ECs, and lymphatic ECs, didn't show such difference between tumor tissues and normal tissues in multiple cancer types. Interestingly, the proportion of total ECs in seven kinds of tumors, including COAD, KICH, KIRC, KIRP, LIHC, LUAD, LUSC, and THCA, was higher than normal tissues, indicating that angiogenesis in these tumor tissues is more active (Fig. S4C).

3.3. Tip-like ECs represent an activated EC subcluster that may promote tumor angiogenesis while inhibit antitumor immune response

Next, we investigated the molecular features of the tip-like ECs. GSVA of the hallmark pathways revealed that tip-like ECs had a higher enrichment score for Notch signaling, Wnt/β-catenin signaling, angiogenesis, and protein secretion pathways, indicating that tip-like ECs represented an activated EC subcluster that promote tumor angiogenesis (Fig. 4A)[15,28,29]. Capillary ECs 2 showed enrichment in inflammation-related pathways, such as inflammatory response and TNF-α signaling (Fig. 4A). By contrast, capillary ECs 1 might be in a resting state. We then performed GO analysis using GSVA and found an enrichment of the gene set that involved in cadherin mediated negative regulation of cell-cell adhesion in tip-like ECs (Fig. 4B; Table S10), indicating that tip-like ECs may facilitate tumor cell growth by inducing vascular permeability [30].

To explore how tip-like ECs affect TME, we conducted CellChat analysis in different cancer types. We found that MIF-CD74 axis was highly enriched between tip-like ECs and immune cells, including macrophages, monocytes, $CD4^+$ T cells, and $CD8^+$ T cells in all six cancer types we analyzed (Fig. 4C-E; Fig. S5A-C). Recent studies have revealed that MIF-CD74 axis could inhibit anti-tumor immune response through recruiting tumor-associated macrophages (TAMs) or directly suppressing T cell activation [31,32]. Therefore, tip-like ECs might inhibit anti-tumor immune response through crosstalk with multiple immune cells. We also found a significantly negative correlation between tip-like ECs and $CD8^+$ T cells in a variety of cancer types, indicating that tip-like ECs might inhibit the infiltration of $CD8^+$ T cells (Fig. S5D). Altogether, tip-like ECs represent an activated EC subcluster which may promote tumor angiogenesis while inhibit anti-tumor immune response.

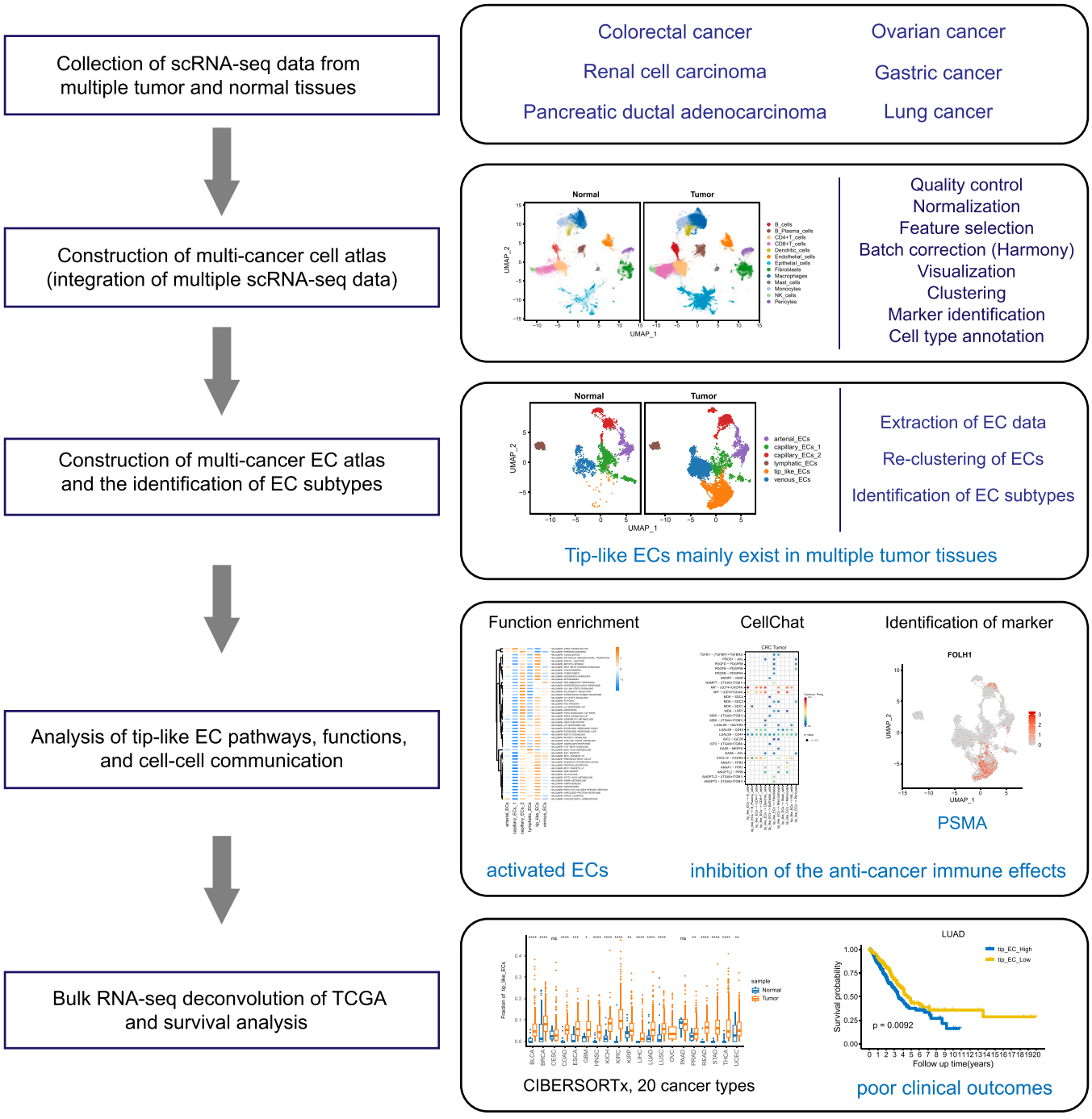

Fig. 1. Workflow of the integrated analysis in this study.

3.4. Tumor cells, stromal cells, and myeloid cells are the main source of pro-angiogenic factors

TME has high levels of pro-angiogenic factors, such as VEGF, placental growth factor (PlGF, encoded by PGF), platelet-derived growth factor (PDGF), and fibroblast growth factor (FGF) [9,30]. Therefore, we performed cell-cell communication analysis to identify the source of these pro-angiogenic factors. Results showed that tumor cells, fibroblasts, myeloid cells, and pericytes could secrete VEGFA or PlGF (Fig. 5A-E; Fig. S6). Further analysis showed that tumor cells and myeloid cells, including macrophages, monocytes, mast cells, and DCs, were the main sources of VEGFA, while pericytes were the major producer of PlGF (Fig. 5F, G).

3.5. High proportion of tip-like ECs is associated with poor clinical outcome in multiple cancer types

To further evaluate the correlation between the proportion of tip-like ECs and patients' overall survival, patients with different cancer types from TCGA database were divided into two groups based on the proportions of tip-like ECs (high or low) for survival analysis. Results showed that high proportion of tip-like ECs was associated

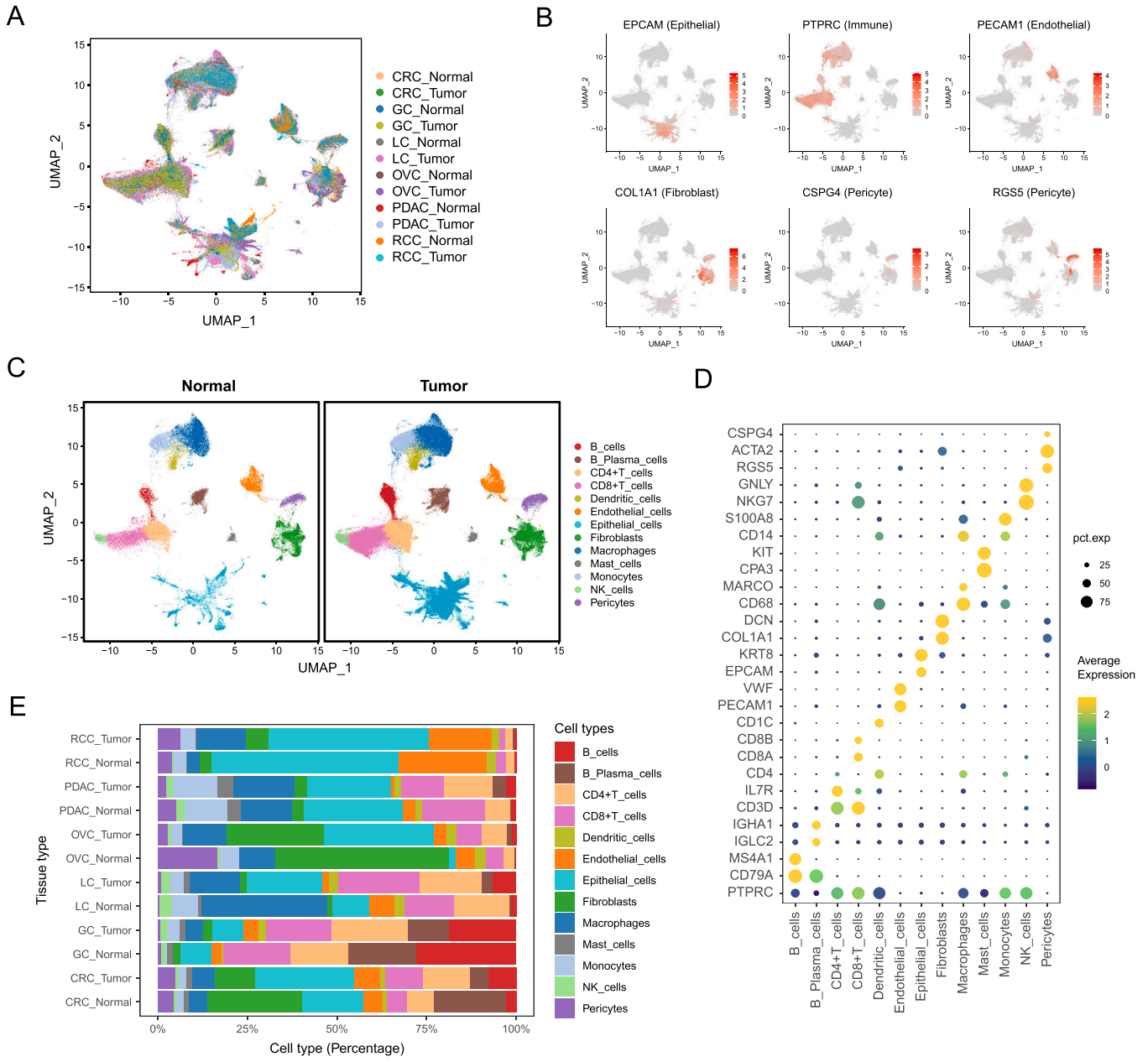

Fig. 2. The integration of scRNA-seq data and construction of multi-cancer cell atlas. A, UMAP representation of individual cells colored by tissue of origin. B, UMAP showing the expression of classical markers for epithelial cells (EPCAM), immune cells (PTPRC/CD45), endothelial cells (PECAM1/CD31), fibroblasts (COL1A1), and pericytes (CSPG2/NG2 and RGS5). C, UMAP visualization of the cell populations across six cancer types. D, Marker gene expression for each cell type in multi-cancer, where dot size and color represent the percentage of marker gene expression (Pct. exp) and the averaged scaled expression (Avg. exp. scale) value, respectively. E, Bar plots to show the proportion of different cell types in each tissue. CRC, colorectal cancer; OVC, ovarian cancers; PDAC, pancreatic ductal adenocarcinoma; GC, gastric cancer; LC, lung cancer; OVC, ovarian cancer; RCC, renal cell carcinoma.

with poor clinical outcome in several cancer cohorts, including LUAD, OV, STAD, CESC, KIRP, BLCA, and UCEC (Fig. 6A-F; Fig. S7; Table S11).

3.6. PSMA is a specific marker for tip-like ECs in non-prostate cancers

The above results indicated that tip-like ECs play an important role in tumor progression and could be used as potential targets for cancer therapy. To ensure precise targeting, we systematically evaluated the specific membrane markers in tip-like ECs. CXCR4 was a commonly used marker for tip ECs, which showed higher expression in tip ECs than other EC subclusters [15,26]. However, as shown in Fig. 7A-C, CXCR4 was also expressed in most immune cells, thus it's not an ideal marker for tip-like ECs. To identify more specific membrane markers for tip-like ECs, we screened all the membrane molecules, trying to find a specific marker for tip-like ECs. First, we screened the genes that were highly expressed in tip-like ECs than other EC subclusers, using a cutoff of $\log_2$ FoldChange > 1 and $p < 0.05$, then we selected the membrane molecules by querying the Uniprot database [33]. Results showed that the specifically highly

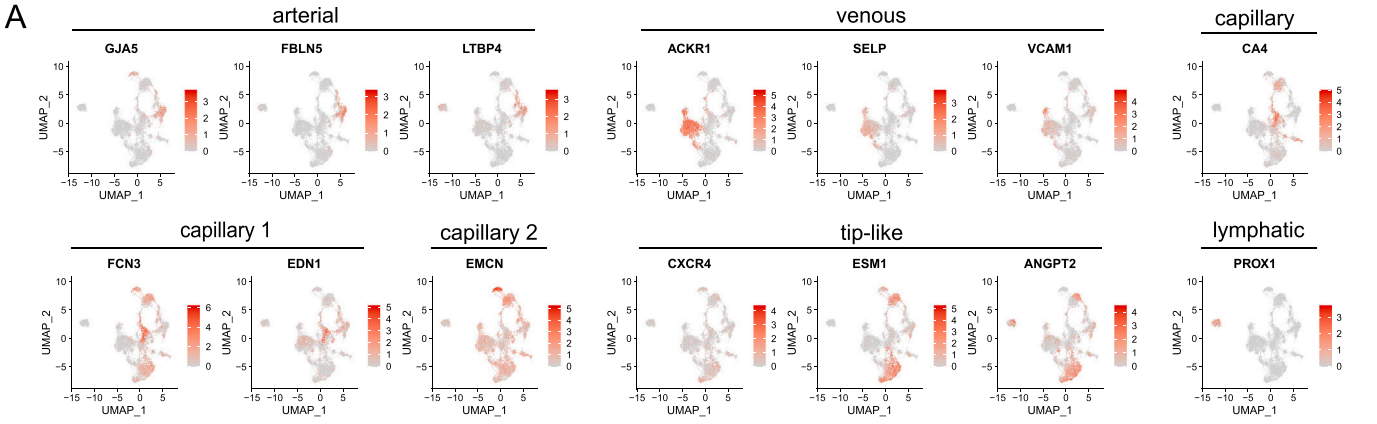

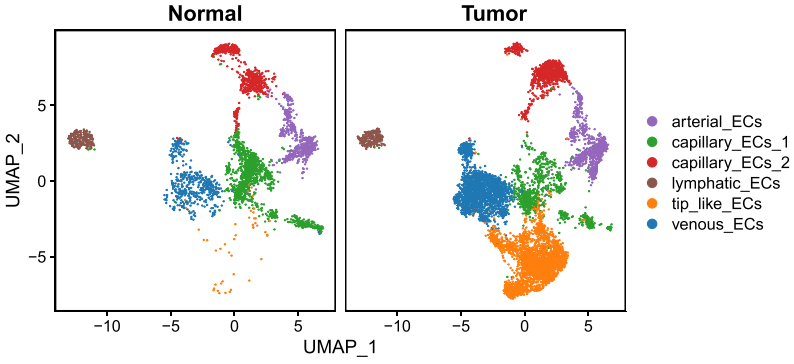

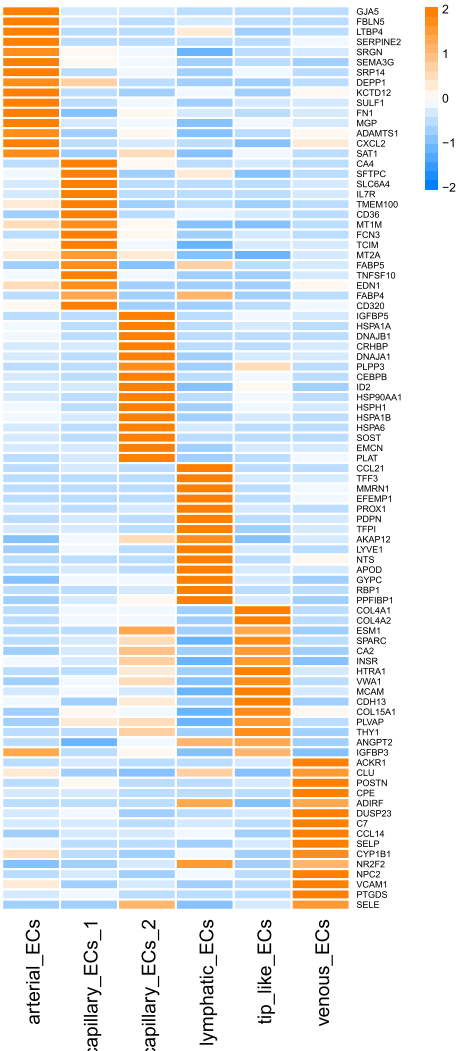

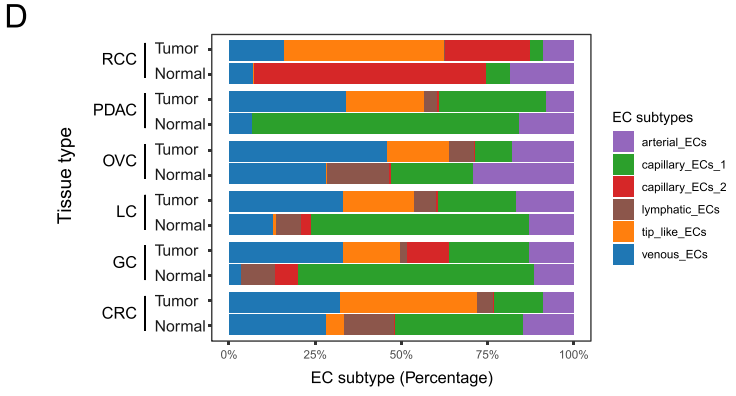

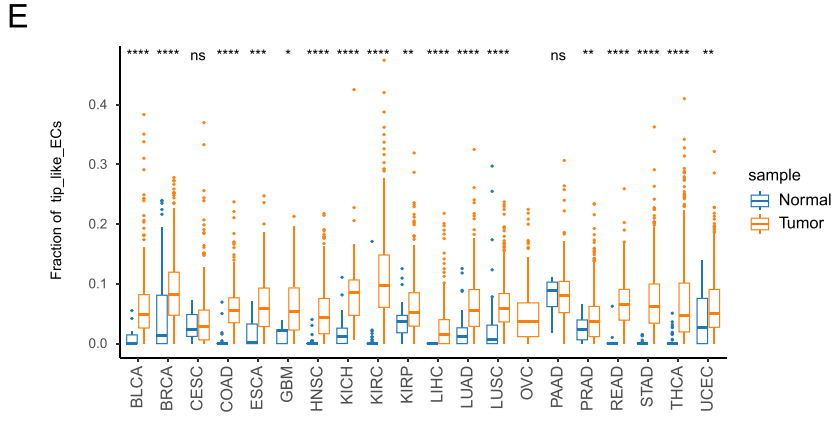

(caption on next page)

Fig. 3. Integrated analysis of single cell and bulk RNA-seq data reveals the differences in EC composition between tumor and normal tissues. A, UMAP plots to show the expression of classical EC markers in EC atlas. B, UMAP visualization of EC subclusters from multiple cancer types. Different EC subclusters are color-coded. C, Heatmap to show the top DEGs (Wilcoxon test) in each EC subcluster. D, Bar plots to show the proportion of different EC subclusters in each tissue. E, The fractions of tip-like ECs between tumor tissues and normal tissues in 20 TCGA cancer types. Comparisons of cellular proportions between tumors and normal tissues for each cancer type were performed using Wilcoxon rank sum test. DEG, differentially expressed genes. BLCA, Bladder Urothelial Carcinoma; BRCA, Breast invasive carcinoma; CESC, Cervical squamous cell carcinoma and endocervical adenocarcinoma; COAD, Colon adenocarcinoma; ESCA, Esophageal carcinoma; GBM, Glioblastoma multiforme; HNSC, Head and Neck squamous cell carcinoma; KICH, Kidney Chromophobe; KIRC, Kidney renal clear cell carcinoma; KIRP, Kidney renal papillary cell carcinoma; LIHC, Liver hepatocellular carcinoma; LUAD, Lung adenocarcinoma; LUSC, Lung squamous cell carcinoma; OV, Ovarian serous cystadenocarcinoma; PAAD, Pancreatic adenocarcinoma; PRAD, Prostate adenocarcinoma; READ, Rectum adenocarcinoma; STAD, Stomach adenocarcinoma; THCA, Thyroid carcinoma; UCEC, Uterine Corpus Endometrial Carcinoma.

expressed membrane molecules in tip-like ECs included CA2, INSR, HTRA1, MCAM, CDH13, PLVAP, THY1, TNFRSF4, LAMA4, PXDN, FOLH1, and EDNRB. After comparing their expression in different EC subclusters, we found that FOLH1 was the only one that was differentially expressed between tip-like ECs and other EC subclusters, with more than one-third of tip-like ECs while less than one-tenth of

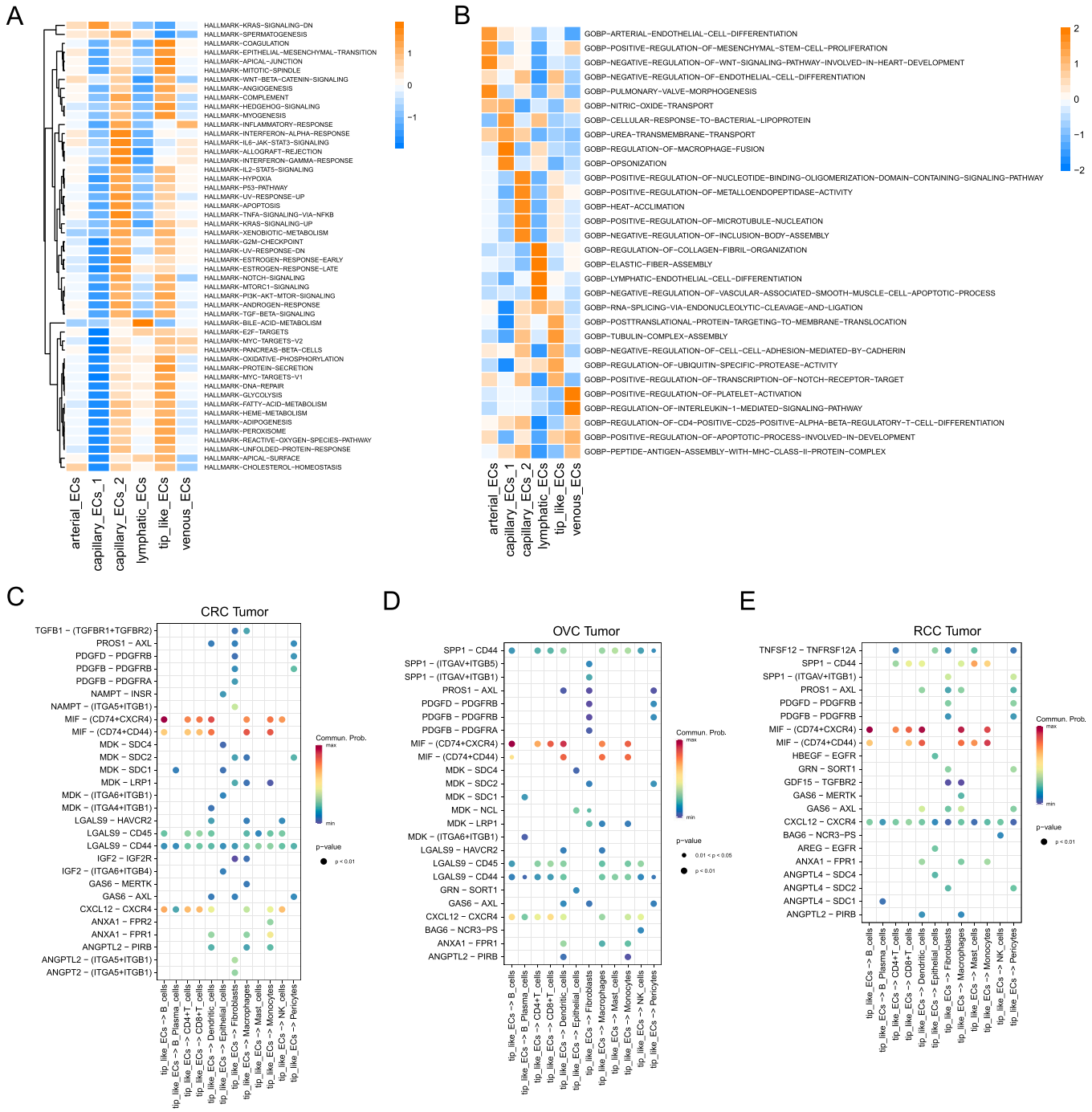

Fig. 4. Tip-like ECs represent an activated EC subcluster that promote tumor angiogenesis while inhibit antitumor immune response. A, Activation of Hallmark pathways (scored per cell by GSVA) in six EC subclusters. B, Heatmap to show the differentially enriched GO terms in each EC subcluster. C-E, Interaction analysis to show the enriched receptor-ligand pairs between tip-like ECs and other cell types in CRC (C), OVC (D), and RCC (E).

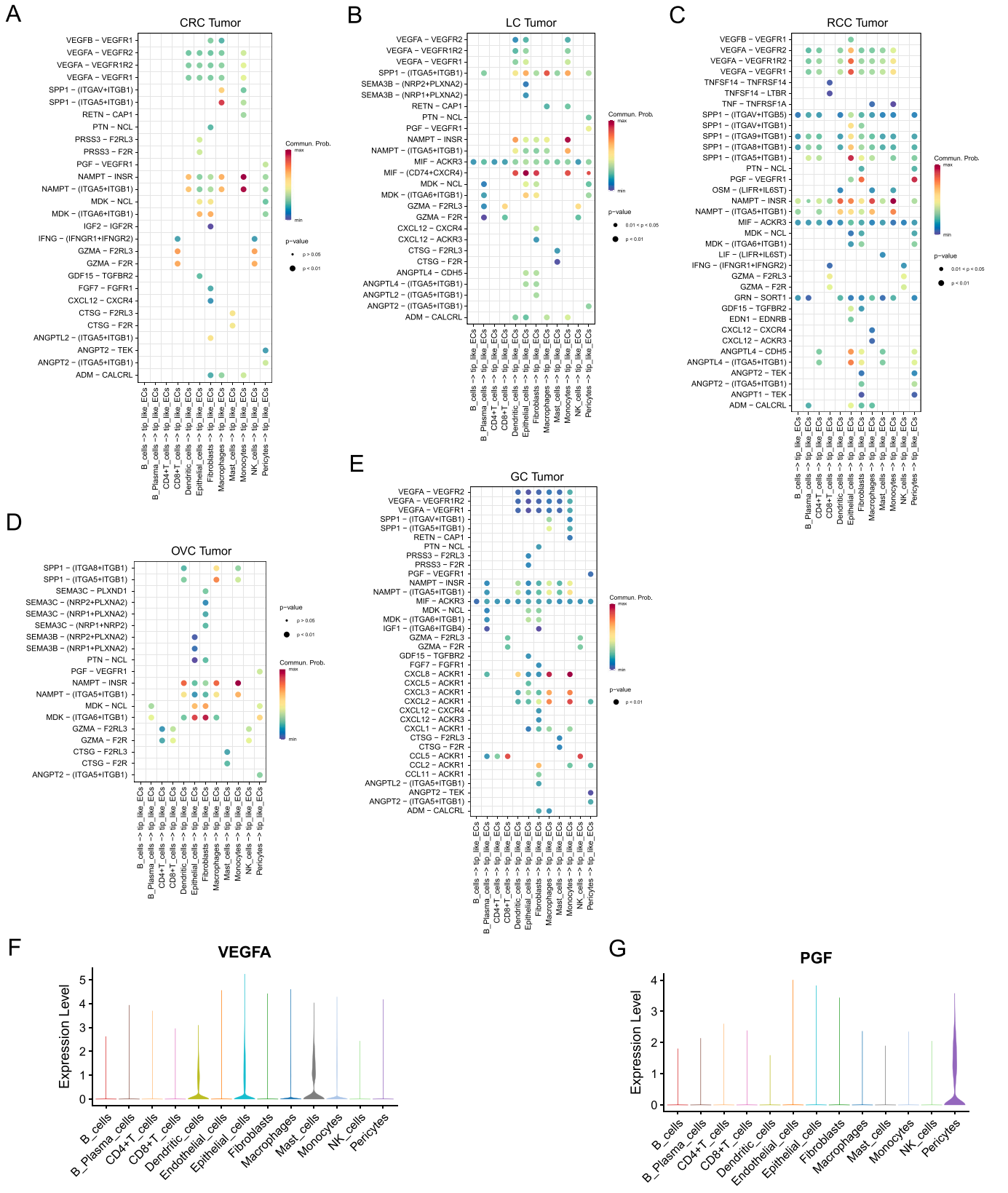

Fig. 5. Tumor cells, stromal cells, and myeloid cells are the main source of pro-angiogenic factors. A-E, Cell-cell communication analysis to show the enriched receptor-ligand pairs between other cell types and tip-like ECs in CRC (A), LC (B), RCC (C), OVC (D), and GC (E). F and G, Violin plots to show the expression levels of VEGFA (F) and PGF (G) in different cell types.

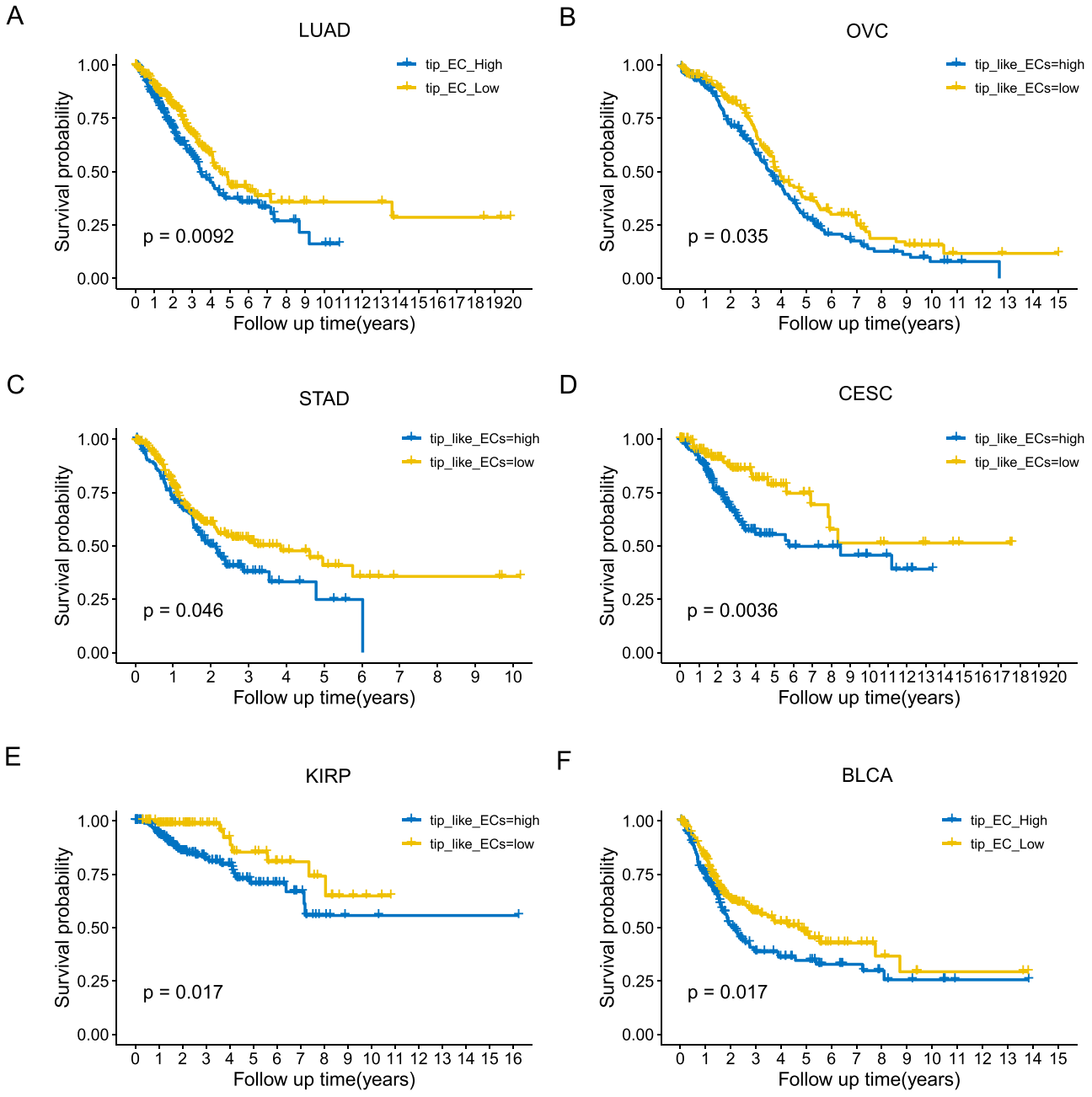

Fig. 6. High proportion of tip-like ECs is associated with poor clinical outcome in multiple cancer types. A-F, Kaplan-Meier plots to depict the survival of patients with high tip-like ECs and low tip-like ECs in LUAD (**A**), OVC (**B**), STAD(**C**), CESC(**D**), KIRP(**E**), and BLCA(**F**). P-values were calculated using log rank test.

other EC subclusters had expression (Fig. 7D, E; Fig. S8B). Moreover, less than 5 % of epithelial cells, immune cells, fibroblasts, and pericytes had FOLH1 expression (Fig. S8A-C). Thus, we proposed that prostate-specific membrane antigen (PSMA, encoded by FOLH1) could be used as a specific marker and therapeutic target for tip-like ECs.

4. Discussion

Tumor blood vessels facilitate tumor growth, metastasis, and immune escape [4,34,35]. Some studies reported increased abundance of tip-like ECs in different single type of tumor tissues, some also explored the molecular characteristics of the tip-like ECs [15,36]. However, few studies compared the phenotypic and molecular characteristics of tip-like ECs in different cancer types.

In this study, we constructed a multi-cancer EC atlas and characterized the heterogeneity of ECs across multiple cancer types. By using integrated single-cell and bulk RNA-seq data, we found that tip-like ECs specifically existed in tumor tissues and could be used as potential targets for the diagnosis and treatment of multiple cancer types. Furthermore, we found that PSMA was a specific membrane marker for tip-like ECs in non-prostate cancers. PSMA is a type II transmembrane glycoprotein with folate hydrolase and N-acetylated-α-linked-acidic dipeptidase activities [37]. PSMA has been

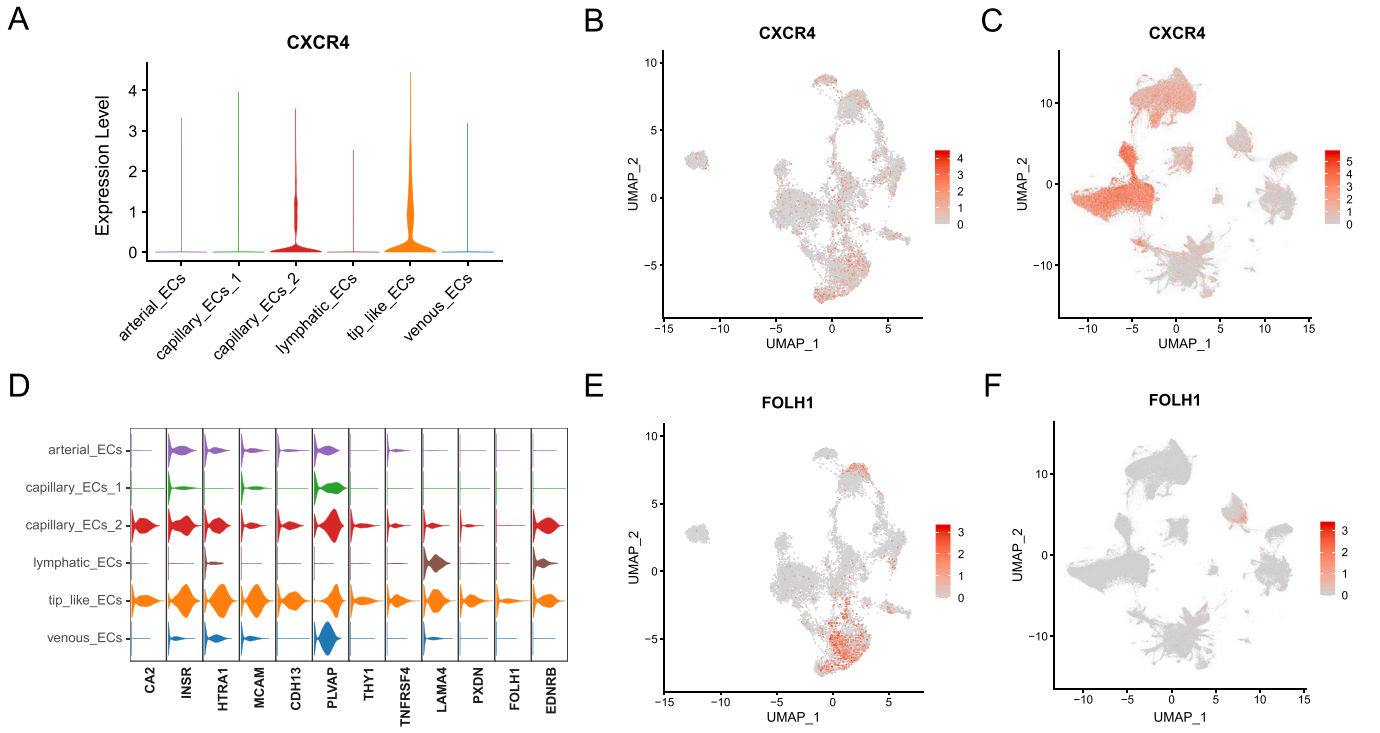

Fig. 7. PSMA is a specific marker for tip-like ECs in non-prostate cancers. A, Violin plots to show the expression levels of CXCR4 in different EC subclusters. B and C, UMAP visualization of cell atlas to reveal the expression of CXCR4 in each EC subcluster (B) and all cell types (C). D, Violin plots to show the expression levels of the highly expressed surface molecules for tip-like ECs in different EC subclusters. E and F, UMAP visualization of cell atlas to reveal the expression of PSMA (FOLH1) in each EC subcluster (E) and all cell types (F).

widely used as a target for the diagnosis and treatment of prostate cancer because of its high expression in prostate cancer cells [38]. Previously, PSMA has also been found to be co-localized with CD34 in tumor vasculature by using immunohistochemical staining in various tumor tissues [39,40]. Since CD34 was considered to be a marker of angiogenic tip cells in human vascular ECs [41], these results confirmed the specific PSMA expression in tumor vasculature in other solid tumors. And PSMA specific positron emission tomography (PET)/computed tomography (CT) has also be applied to identify other solid tumors, such as RCC and hepatocellular carcinoma, because of its specific expressed in tumor vasculature [42,43]. Through both in vivo and in vitro experiments, Conway et al. found that PSMA could modify laminin downstream of MMP-2 to augment integrin β1 activation and angiogenesis, which confirmed the function of PSMA in angiogenesis [44,45]. In our study, we found that PSMA could be used as a marker of tip-like ECs, which specifically exist in tumor tissues. Our study provides more molecular basis for the application of PSMA-based diagnostic imaging in non-prostate cancers.

Besides the identification of their specific existence in tumor tissues, we also decoded the molecular features of tip-like ECs in multiple cancer types, which showed highly consistent phenotype. Tip-like ECs represented activated EC subcluster that promote tumor angiogenesis and play important roles in shaping TME. Our results showed that tip-like ECs might recruit TAMs or directly inhibit T-cell activation via MIF-CD74 axis, resulting in suppressed anti-tumor immune response. MIF has been shown to contribute to tumor immune escape by counteracting $CD8^+$ T cell mediated immune surveillance [46]. Vascular expression of PSMA in various tumor types has also been shown to be associated with tumor progression and poor prognosis [40,47,48], and we also found that high proportion of tip-like ECs was correlated with poor clinical outcomes in several cancer cohorts. Thus, tip-like ECs could be used as novel therapeutic targets, with PSMA as the specific membrane molecule for targeting in non-prostate cancers. Our scRNA-seq analysis data showed that PSMA was expressed in 37.4 % of tip-like ECs and 19.3 % of tumor ECs (Fig. S8B and C). The relative low proportion of tip-like ECs with PSMA expression might be partially due to the low coverage of transcripts sequenced by scRNA-seq process with the high cell throughputs [49,50].

Crosstalk between ECs and other cell types could facilitate tumor angiogenesis and resistance to anti-angiogenic therapy [9]. We found that various pro-angiogenic growth factors existed in TME, and tumor cells and myeloid cells such as macrophages, monocytes, mast cells, and DCs, were the main sources of VEGFA, while pericytes were the major producers of PlGF. These results indicate that myeloid cells and pericytes play important roles in tumor angiogenesis. In our study, we found that in RCC and CRC, the proportion of tip-like ECs was higher than other caner types, and since our cell-cell communication analysis data showed that in RCC and CRC, especially RCC, there have much higher levels of VEGF and PlGF, these results indicated that the tip-like ECs may receive stronger proangiogenic signals in these cancer types. Thus, we think tip-like ECs with PSMA may be most useful for targeting a subset of cancer types such as RCC.

Most studies on the characteristics of tip cells were performed in single cancer type. For example, one study found that tip cells only existed in the tumor tissue of lung cancer, but not in normal lung tissues [15]. Tip ECs were considered as the key phenotype in sprouting angiogenesis, and in papillary thyroid carcinoma, it was found that the expression of several transcription factors that were associated with endothelial migration and sprouting, such as ZEB1,

HOXB5 and STAT family (STAT1, STAT2), were upregulated in tip cells [51]. In our study, we revealed the common features of tip-like ECs in multiple cancer types. We found that tip-like ECs mainly exist in various tumor tissues but barely exist in normal tissues. Moreover, we found that tip-like ECs could promote tumor angiogenesis and inhibit anti-tumor immune response, and their function was consistent among different cancer types. Finally, we identified that PSMA could be used as a specific marker for tip-like ECs, confirming the rationality to use it as a target for diagnosis and treatment of non-prostate cancers.

However, our study also had some limitations. We only analyzed scRNA-seq data from six cancer types. Analysis in more cancer types will definitely improve the accuracy of current results. Furthermore, results in this study were obtained through integrated analysis of single-cell and bulk RNA-seq data, the proposed features and functions of tip-like ECs need be validated by experiments.

In summary, we revealed the difference of ECs between tumor tissues and normal tissues in multiple cancer types via integrated analysis of single-cell and bulk RNA-seq data. We found that tip-like ECs were the main differential subcluster of ECs between tumors and normal tissues. Tip-like ECs represented an activated EC subcluster that could promote tumor angiogenesis and influence the tumor immune microenvironment. In addition, high proportion of tip-like ECs was correlated with poor clinical outcomes in multiple cancer types. Furthermore, we identified that PSMA could be used as a specific marker for tip-like ECs, which confirmed the rationality to use it as a target for the diagnosis and treatment of non-prostate cancers.

Funding

This study was supported by the National Natural Science Foundation of China (No. 82173204; 82203633; 82202933; 82201774), the Innovation Capability Support Program of Shaanxi Province, China (2020PT-021; 2021TD-39), the Natural Science Basic Research Program of Shaanxi Province, China (2022JZ-62), and the Fundamental Research Funds for the Central Universities, China (G2021KY05102).

CRediT authorship contribution statement

Jiayu Zhang: Conceptualization, Formal analysis, Writing - original draft, Writing - review & editing. **Tong Lu:** Data curation, Visualization, Writing - original draft. **Shiqi Lu:** Methodology, Investigation, Writing - original draft. **Shuaijun Ma:** Data curation, Software. **Donghui Han:** Visualization, Funding acquisition. **Keying Zhang:** Methodology, Funding acquisition. **Chao Xu:** Software, Investigation. **Shaojie Liu:** Writing - review & editing. **Lunbiao Gan:** Formal analysis. **Xinjie Wu:** Methodology, Investigation. **Fa Yang:** Conceptualization, Funding acquisition. **Weihong Wen:** Writing - review & editing, Funding acquisition. **Weijun Qin:** Supervision, Project administration, Funding acquisition.

Data availability

The scRNA-seq data were obtained from https://lambrechtslab.sites.vib.be/en/data-access and the Gene Expression Omnibus (GEO, RRID: SCR_005012) with reference numbers GSE155698, GSE159115, and GSE167297. TCGA bulk RNA-seq data with FPKM values and clinical data were obtained from the UCSC Xena platform [52].

All R packages used are available online. Customized code for data analysis and plotting are available on GitHub (https://github.com/jiayu2022/Multi-Cancer-EC-Atlas).

Declaration of Competing Interest

The authors declare that they have no known competing financial interests or personal relationships that could have appeared to influence the work reported in this paper.

Acknowledgments

We thank Dr. Jianming Zeng (Faculty of Health Sciences, University of Macau, China) and all the members of his bioinformatics team, biotrainee, for generously sharing their experience and codes.

Ethics approval and consent to participate

Not applicable.

Consent for publication

Not applicable.

Appendix A. Supporting information

Supplementary data associated with this article can be found in the online version at doi:10.1016/j.csbj.2022.12.049.

References

[1] Anderson NM, Simon MC. The tumor microenvironment. Curr Biol 2020;30(16):R921–5.
[2] La Porta S, Roth L, Singhal M, Mogler C, Spegg C, Schieb B, et al. Endothelial Tie1-mediated angiogenesis and vascular abnormalization promote tumor progression and metastasis. J Clin Invest 2018;128(2):834–45.
[3] Kumar S, Bar-Lev L, Sharife H, Grunewald M, Mogilevsky M, Licht T, et al. Identification of vascular cues contributing to cancer cell stemness and function. Angiogenesis 2022;25(3):355–71.
[4] Huijbers EJM, Khan KA, Kerbel RS, Griffioen AW. Tumors resurrect an embryonic vascular program to escape immunity. Sci Immunol 2022;7(67):eabm6388.
[5] Young MD, Mitchell TJ, Vieira Braga FA, Tran MGB, Stewart BJ, Ferdinand JR, et al. Single-cell transcriptomes from human kidneys reveal the cellular identity of renal tumors. Science 2018;361(6402):594–9.
[6] Griffioen AW, Damen CA, Martinotti S, Blijham GH, Groenewegen G. Endothelial intercellular adhesion molecule-1 expression is suppressed in human malignancies: the role of angiogenic factors. Cancer Res 1996;56(5):1111–7.
[7] Griffioen AW, Damen CA, Blijham GH, Groenewegen G. Tumor angiogenesis is accompanied by a decreased inflammatory response of tumor-associated endothelium. Blood 1996;88(2):667–73.
[8] Dirkx AE, Oude Egbrink MG, Kuijpers MJ, van der Niet ST, Heijnen VV, Boumater Steege JC, et al. Tumor angiogenesis modulates leukocyte-vessel wall interactions in vivo by reducing endothelial adhesion molecule expression. Cancer Res 2003;63(9):2322–9.
[9] Huang M, Lin Y, Wang C, Deng L, Chen M, Assaraf YG, et al. New insights into antiangiogenic therapy resistance in cancer: Mechanisms and therapeutic aspects. Drug Resist Updat 2022;64:100849.
[10] Jayson GC, Kerbel R, Ellis LM, Harris AL. Antiangiogenic therapy in oncology: current status and future directions. Lancet 2016;388(10043):518–29.
[11] Bejarano L, Jordão MJC, Joyce JA. Therapeutic targeting of the tumor microenvironment. Cancer Discov 2021;11(4):933–59.
[12] Eelen G, Treps L, Li X, Carmeliet P. Basic and therapeutic aspects of angiogenesis updated. Circ Res 2020;127(2):310–29.
[13] Cignarella A, Fadini GP, Bolego C, Trevisi L, Boscaro C, Sang V, et al. Clinical efficacy and safety of angiogenesis inhibitors: sex differences and current challenges. Cardiovasc Res 2022;118(4):988–1003.
[14] Zhao Q, Eichten A, Parveen A, Adler C, Huang Y, Wang W, et al. Single-cell transcriptome analyses reveal endothelial cell heterogeneity in tumors and changes following antiangiogenic treatment. Cancer Res 2018;78(9):2370–82.
[15] Goveia J, Rohlenova K, Taverna F, Treps L, Conradi LC, Pircher A, et al. An integrated gene expression landscape profiling approach to identify lung tumor

endothelial cell heterogeneity and angiogenic candidates. Cancer Cell 2020;37(1):21–36. e13.
[16] Heidegger I, Fotakis G, Offermann A, Goveia J, Daum S, Salcher S, et al. Comprehensive characterization of the prostate tumor microenvironment identifies CXCR4/CXCL12 crosstalk as a novel antiangiogenic therapeutic target in prostate cancer. Mol Cancer 2022;21(1):132.
[17] Qian J, Olbrecht S, Boeckx B, Vos H, Laoui D. Etlioglu,et al. A pan-cancer blueprint of the heterogeneous tumor microenvironment revealed by single-cell profiling. Cell Res 2020;30(9):745–62.
[18] Steele NG, Carpenter ES, Kemp SB, Sirihorachai VR, The S. L. Delrosario, et al. Multimodal mapping of the tumor and peripheral blood immune landscape in human pancreatic cancer. Nat Cancer 2020;1(11):1097–112.
[19] Zhang Y, Narayanan SP, Mannan R, Raskind G, Wang X. P. Vats, et al. Single-cell analyses of renal cell cancers reveal insights into tumor microenvironment, cell of origin, and therapy response. Proc Natl Acad Sci U S A 2021;118(24).
[20] Jeong HY, Ham IH, Lee SH, Ryu D, Son SY. S.U. Han, et al. Spatially distinct reprogramming of the tumor microenvironment based on tumor invasion in diffuse-type gastric cancers. Clin Cancer Res 2021;27(23):6529–42.
[21] Hao Y, Hao S, Andersen-Nissen E, Mauck 3rd WM, Zheng S, Butler A, et al. Integrated analysis of multimodal single-cell data. Cell 2021;184(13):3573–87. e29.
[22] Korsunsky I, Millard N, Fan J, Slowikowski K, Zhang F, Wei K, et al. Fast, sensitive and accurate integration of single-cell data with Harmony. Nat Methods 2019;16(12):1289–96.
[23] Hanzelmann S, Castelo R, Guinney J. GSVA: gene set variation analysis for microarray and RNA-seq data. BMC Bioinformatics 2013;14:7.
[24] Jin S, Guerrero-Juarez CF, Zhang L, Chang I, Ramos R, Kuan CH, et al. Inference and analysis of cell-cell communication using. CellChat. Nat Commun 2021;12(1):1088.
[25] Newman AM, Steen CB, Liu CL, Gentles AJ, Chaudhuri AA, Scherer F, et al. Determining cell type abundance and expression from bulk tissues with digital cytometry. Nat Biotechnol 2019;37(7):773–82.
[26] Strasser GA, Kaminker JS, Tessier-Lavigne M. Microarray analysis of retinal endothelial tip cells identifies CXCR4 as a mediator of tip cell morphology and branching. Blood 2010;115(24):5102–10.
[27] del Toro R, Prahst C, Mathivet T, Siegfried G, Kaminker JS, Larrivee B, et al. Identification and functional analysis of endothelial tip cell-enriched genes. Blood 2010;116(19):4025–33.
[28] Zhou B, Lin W, Long Y, Yang Y, Zhang H, Wu K, et al. Notch signaling pathway: architecture, disease, and therapeutics. Signal Transduct Target Ther 2022;7(1):95.
[29] Liu J, Xiao Q, Xiao J, Niu C, Li Y, Zhang X, et al. Wnt/beta-catenin signalling: function, biological mechanisms, and therapeutic opportunities. Signal Transduct Target Ther 2022;7(1):3.
[30] Yang Y, Cao Y. The impact of VEGF on cancer metastasis and systemic disease. Semin Cancer Biol 2022;86(Pt 3):251–61.
[31] Klemke L, De Oliveira T, Witt D, Winkler N, Bohnenberger H, Bucala R, et al. Hsp90-stabilized MIF supports tumor progression via macrophage recruitment and angiogenesis in colorectal cancer. Cell Death Dis 2021;12(2):155.
[32] Balogh KN, Templeton DJ, Cross JV. Macrophage Migration Inhibitory Factor protects cancer cells from immunogenic cell death and impairs anti-tumor immune responses. PLoS One 2018;13(6):e0197702.
[33] UniProt C. UniProt: the universal protein knowledgebase in 2021. Nucleic Acids Res 2021;49(D1):D480–9.
[34] Cantelmo AR, Conradi LC, Brajic A, Goveia J, Kalucka J, Pircher A, et al. Inhibition of the glycolytic activator PFKFB3 in endothelium induces tumor vessel normalization, impairs metastasis, and improves chemotherapy. Cancer Cell 2016;30(6):968–85.
[35] Ando T, Tai-Nagara I, Sugiura Y, Kusumoto D, Okabayashi K, Kido Y, et al. Tumor-specific interendothelial adhesion mediated by FLRT2 facilitates cancer aggressiveness. J Clin Invest 2022;132(6).
[36] Xing X, Yang F, Huang Q, Guo H, Li J, Qiu M, et al. Decoding the multicellular ecosystem of lung adenocarcinoma manifested as pulmonary subsolid nodules by single-cell RNA sequencing. Sci Adv 2021;7(5).
[37] He Y, Xu W, Xiao YT, Huang H, Gu D, Ren S, et al. Targeting signaling pathways in prostate cancer: mechanisms and clinical trials. Signal Transduct Target Ther 2022;7(1):198.
[38] Lawhn-Heath C, Salavati A, Behr SC, Rowe SP, Calais J, Fendler WP, et al. Prostate-specific membrane antigen PET in prostate cancer. Radiology 2021;299(2):248–60.
[39] Chang SS, Reuter VE, Heston WD, Bander NH, Grauer LS, Gaudin PB, et al. Five different anti-prostate-specific membrane antigen (PSMA) antibodies confirm PSMA expression in tumor-associated neovasculature. Cancer Res 1999;59(13):3192–8.
[40] Tanjore Ramanathan J, Lehtipuro S, Sihto H, Tovari J, Reiniger L, Teglasi V, et al. Prostate-specific membrane antigen expression in the vasculature of primary lung carcinomas associates with faster metastatic dissemination to the brain. J Cell Mol Med 2020;24(12):6916–27.
[41] Siemerink MJ, Klaassen I, Vogels IM, Griffioen AW, Van Noorden CJ, Schlingemann RO, et al. CD34 marks angiogenic tip cells in human vascular endothelial cell cultures. Angiogenesis 2012;15(1):151–63.
[42] Li Y, Zheng R, Zhang Y, Huang C, Tian L, Liu R, et al. Special issue "The advance of solid tumor research in China": 68Ga-PSMA-11 PET/CT for evaluating primary and metastatic lesions in different histological subtypes of renal cell carcinoma. Int J Cancer 2023;152(1):42–50.
[43] Hirmas N, Leyh C, Sraieb M, Barbato F, Schaarschmidt BM, Umutlu L, et al. (68)Ga-PSMA-11 PET/CT improves tumor detection and impacts management in patients with hepatocellular carcinoma. J Nucl Med 2021;62(9):1235–41.
[44] Conway RE, Joiner K, Patterson A, Bourgeois D, Rampp R, Hannah BC, et al. Prostate specific membrane antigen produces pro-angiogenic laminin peptides downstream of matrix metalloprotease-2. Angiogenesis 2013;16(4):847–60.
[45] Conway RE, Petrovic N, Li Z, Heston W, Wu D, Shapiro LH, et al. Prostate-specific membrane antigen regulates angiogenesis by modulating integrin signal transduction. Mol Cell Biol 2006;26(14):5310–24.
[46] Mittelbronn M, Platten M, Zeiner P, Dombrowski Y, Frank B, Zachskorn C, et al. Macrophage migration inhibitory factor (MIF) expression in human malignant gliomas contributes to immune escape and tumour progression. Acta Neuropathol 2011;122(3):353–65.
[47] Li Y, Zhang K, Yang F, Jiao D, Li M, Zhao X, et al. Prognostic value of vascular-expressed PSMA and CD248 in urothelial carcinoma of the bladder. Front Oncol 2021;11:771036.
[48] Jiao D, Li Y, Yang F, Han D, Wu J, Shi S, et al. Expression of prostate-specific membrane antigen in tumor-associated vasculature predicts poor prognosis in hepatocellular carcinoma. Clin Transl Gastroenterol 2019;10(5):1–7.
[49] Hagemann-Jensen M, Ziegenhain C, Sandberg R. Scalable single-cell RNA sequencing from full transcripts with Smart-seq3xpress. Nat Biotechnol 2022;40(10):1452–7.
[50] Mereu E, Lafzi A, Moutinho C, Ziegenhain C, McCarthy DJ, Alvarez-Varela A, et al. Benchmarking single-cell RNA-sequencing protocols for cell atlas projects. Nat Biotechnol 2020;38(6):747–55.
[51] Pu W, Shi X, Yu P, Zhang M, Liu Z, Tan L, et al. Single-cell transcriptomic analysis of the tumor ecosystems underlying initiation and progression of papillary thyroid carcinoma. Nat Commun 2021;12(1):6058.
[52] Goldman MJ, Craft B, Hastie M, Repecka K, McDade F, Kamath A, et al. Visualizing and interpreting cancer genomics data via the Xena platform. Nat Biotechnol 2020;38(6):675–8.